Overcoming the Low Relaxivity of Gadofosveset at High Field with Spin Locking

O. C. Richardson,[1] M. L. J. Scott,[2] S. F. Tanner,[1] J. C. Waterton,[2] and D. L. Buckley[1]*

The contrast agent gadofosveset, which binds reversibly to serum albumin, has a high longitudinal relaxivity at lower magnetic fields (≤ 3.0 T) but a much lower relaxivity at high fields. Spin locking is sensitive to macromolecular content; it is hypothesized that combining this technique with the albumin-binding properties of gadofosveset may enable increased relaxivity at high fields. In vitro measurements at 4.7 T found significantly higher spin-lock relaxation rates, $R_{1\rho}$ ($1/T_{1\rho}$), when gadofosveset was serum albumin-bound than when unbound. $R_{1\rho}$ values for a nonbinding contrast agent (gadopentetate dimeglumine) in serum albumin were similar to those for unbound gadofosveset. R_2 ($1/T_2$) values were also significantly higher at 4.7 T for serum albumin-bound gadofosveset than for unbound. Spin locking at high field generates significantly higher relaxation rates for gadofosveset than conventional contrast agents and may provide a method for differentiating free and bound molecules at these field strengths. Magn Reson Med 68:1234–1238, 2012. © 2011 Wiley Periodicals, Inc.

Key words: gadofosveset; $T_{1\rho}$; spin locking; relaxivity

The clinically approved contrast agent gadofosveset trisodium (Ablavar, Lantheus Medical Imaging, N Billerica, MA, previously marketed as Vasovist, Schering AG, Germany) is a small-molecule gadolinium (Gd) chelate that acquires macromolecular properties on binding to serum albumin (SA). The gadofosveset molecule consists of a stable gadopentetate core with a phosphodiester linkage to a lipophilic albumin-binding group (1). Over 90% of the agent binds at low concentrations in human serum (2), with a lower binding fraction observed at higher gadofosveset concentrations (3) and in other species (4). The binding process increases the effective molecular weight of gadofosveset from 957 Da to 68 kDa (5), reducing its extravasation rate and prolonging its excretion time, making the agent well suited to angiography (6).

The large bound molecule has a lower tumbling rate and longer rotational correlation time (3), which facilitates a substantially (up to 10-fold) higher longitudinal relaxivity at low magnetic field strengths (4). The longitudinal relaxivity of the bound gadofosveset molecule ($r_{1\text{bound}}$) peaks at around 0.5 T and decreases rapidly with increasing field strengths (7). The longitudinal relaxivity of the free (unbound) gadofosveset molecule ($r_{1\text{free}}$) is slightly higher than conventional small-molecule Gd-based agents such as gadopentetate and shows only a moderate decrease with field strength (8).

The observed longitudinal relaxivity of gadofosveset ($r_{1\text{obs}}$) includes contributions from both the bound and free molecules and is influenced by binding fraction and field strength. The nonlinear relationship between $r_{1\text{obs}}$ and gadofosveset concentration at low field strengths can be modeled (7), although a linear approximation may suffice at low concentrations (8). At 3 T, $r_{1\text{obs}}$ in plasma is still over twice that of most other clinically approved Gd-based agents (8); at higher fields, $r_{1\text{bound}}$ and $r_{1\text{free}}$ converge (9) to give a value of $r_{1\text{obs}}$ similar to conventional Gd-based agents. Regardless of the reduction in relaxivity, the unique kinetic properties of gadofosveset resulting from its binding to albumin are displayed at all field strengths. An alternative contrast mechanism that provides high gadofosveset relaxivity at high fields may be required to fully exploit these properties.

Spin locking (SL), first described as an imaging technique in 1985 (10) but investigated in NMR prior to this (11), involves the application of a 90° excitation pulse followed by an RF pulse (phase shifted by 90° to the excitation pulse), applied for a duration of time (spin-lock time, TSL), which locks the spins in the rotating frame of reference. Relaxation of the magnetization in the presence of this SL field (B_{1L}) is characterized by the time constant $T_{1\rho}$. The SL pulse may be followed by a 90° pulse (phase shifted by 180° to the original excitation pulse) and an imaging sequence, or a 180° pulse and readout (12). $T_{1\rho}$ is influenced by the strength of the SL field, which is commonly in the µT (low kHz) range, rather than the main magnetic field (B_0). As a result, the image contrast generated by SL is equivalent to image contrast obtained at low magnetic fields, with the advantage that a high signal-to-noise ratio may be maintained (13). It should be noted that the SL RF pulse may contribute significantly to patient-specific absorption rate (SAR), particularly at high B_0 as SAR is proportional to the product of B_0^2, B_{1L}^2 and the ratio of TSL to TR (10).

The interaction times associated with SL at very low field strengths give this technique an increased sensitivity to proteins and other macromolecules (14). This correlation between signal intensity (SI) and tissue protein has been utilized as a potential biomarker for response to tumor therapy, including treatment designed to reduce protein synthesis (15) and gene therapy resulting in reduced protein content due to cell death (16). The

[1]Division of Medical Physics, University of Leeds, Leeds, UK.

[2]Imaging, Personalised Healthcare and Biomarkers, AstraZeneca, Macclesfield, Cheshire, United Kingdom.

*Correspondence to: David L. Buckley, Ph.D., Division of Medical Physics, University of Leeds, Room 8.001, Worsley Building, Clarendon Way, Leeds, LS2 9JT, UK. E-mail: D.L.Buckley@leeds.ac.uk

clinical potential of SL has also been highlighted in a study of injured myocardium (17) and the assessment of brain plaque composition in early-onset Alzheimer's disease (18).

Small-molecule Gd-based contrast agents have been used in combination with SL to provide improved myocardium–blood contrast (17,19) and in the assessment of articular cartilage (20). SL after injection of gadopentetate has also been shown to improve tumor contrast in patients with glioma (14). A literature search (August 2011) found no published studies assessing the effect of gadofosveset on $T_{1\rho}$.

The purpose of this study was to determine the potential impact of albumin binding on $T_{1\rho}$ for in vitro gadofosveset solutions at a high B_0 field strength. It was hypothesized that by combining the macromolecular sensitivity of SL with the albumin-binding affinity of gadofosveset a large contrast shift may be achieved at field strengths where the T_1 effects of gadofosveset are very similar to those of conventional Gd-based agents. In addition, it may be possible to use this technique to generate a measurable difference in the relaxation properties of bound and unbound agent.

Tissue $T_{1\rho}$ values fall between T_1 and T_2, with $T_{1\rho} \rightarrow T_2$ as $B_{1L} \rightarrow 0$ (21). Conventionally, $B_{1L} \ll B_0$ therefore $T_{1\rho}$ may be expected to be close to T_2. As the transverse relaxivity of bound gadofosveset is known to remain high at all relevant field strengths (9), and as T_2 values are known to be sensitive to tissue macromolecules (22), a further aspect of the study was to investigate whether the potential benefits of $T_{1\rho}$ contrast could also be achieved using T_2 contrast.

METHODS

Solutions

In vitro solutions of gadofosveset (Vasovist) were prepared using phosphate-buffered saline (PBS, dry powder reconstituted with deionized water, pH = 7.4, Sigma Aldrich, St Louis, MO), to replicate the unbound state, and bovine SA (BSA, Cohn fraction V lyophilized powder, Sigma Aldrich, 4.5% w/v in PBS), to replicate a combination of bound and unbound molecules similar to that found in humans. Stock solutions were created at a gadofosveset concentration of 10 mM, and serially diluted to produce further solutions at 5.0, 3.0, 2.0, 1.5, 1.0, 0.75, 0.5, and 0.25 mM. Solutions of PBS and BSA without contrast agent (0 mM) were also assessed. In order to separate the influence of the macromolecular solution from that of Gd, an equivalent set of solutions of the nonbinding contrast agent gadopentetate dimeglumine (Magnevist, Bayer Healthcare Pharmaceuticals, Germany) in BSA (4.5% w/v) were also created using the same method. Prior to scanning at 4.7 T, all solutions were heated to 37°C in a water bath; this temperature was maintained during scanning with warm air flow and verified with a fiber optic temperature probe in an adjacent water tube. At 0.5 T, samples were heated to 37°C and the temperature monitored with an integral heating system.

Data Acquisition: $T_{1\rho}$

Tubes were placed vertically in a cylindrical cradle of diameter 60 mm and inserted into a 63 mm quad coil in a horizontal bore 4.7 T magnet with Bruker console running ParaVision 5.1 software (Bruker BioSpin MRI GmbH, Ettlingen, Germany). SL was achieved using a B_{1L} pulse value of 90 µT (3.8 kHz), applied for 14 durations (TSL): 0.01, 0.05, 0.1, 0.5, 1.0, 5.0, 12.5, 25.0, 50.0, 75.0, 100.0, 125.0, 150.0, and 200.0 ms. This was followed by a rapid acquisition with relaxation enhancement (RARE) readout, using a coronal (horizontal) slice of thickness 1 mm. The acquisition parameters were: TR = 2000 ms; TE = 10 ms; field of view = 60 × 60 mm; matrix size = 128 × 128 pixels; RARE factor = 2; averages = 1; centric encoding. No spoiler gradients were applied between repetitions.

Data Acquisition: T_1 and T_2

T_1 and T_2 values at 4.7 T were measured using a RARE saturation recovery imaging sequence without the preparatory SL pulse. Tubes were placed horizontally in the cradle and coil described previously and a single axial (vertical) slice used. The acquisition parameters for T_1 were: recovery times = 57.2, 68.5, 78.5, 88.5, 103.5, 183.5, 283.5, and 383.5 ms; TE = 11 ms. For T_2, TE ranged between 11 and 66 ms; TR (BSA) = 2000 ms; TR (PBS) = 8000 ms. Additional parameters common to all: field of view = 60 × 60 mm^2; matrix size = 256 × 256 pixels; RARE factor = 2; averages = 1; centric encoding; slice thickness = 1 mm.

T_1 and T_2 measurements at 0.5 T were made on a Maran NMR spectrometer (Oxford Instruments, Abingdon, UK) utilizing a 20-MHz permanent magnet attached to a thermocouple heating mechanism and a PC running standard system software. T_1 was measured using an inversion recovery sequence, with 20 log incremental inversion time recovery steps and 16 scans. TR was initially estimated for a test scan and then set to at least five times the expected final T_1 value. T_2 measurements were made using a standard Carr-Purcell-Meiboom-Gill sequence, with 1000 TE values.

Model Fitting

On the images acquired at 4.7 T, circular regions of interest were drawn within each tube and the mean SI of each region of interest measured using ImageJ software (v1.42q, Rasband, W.S., ImageJ, U. S. National Institutes of Health, Bethesda, MD; http://imagej.nih.gov/ij/, 1997–2011). SI values were adjusted for noise bias using a simple Rician correction (23), based on mean standard deviations of four background regions in each image. Fitting of $R_{1\rho}$ followed a nonlinear three-parameter fit suggested by Engelhardt and Johnson (24) using MATLAB (v7.9, MathWorks, Natick, MA) to determine the fully recovered SI (S_0) values and relaxation rates ($1/T_{1\rho}$), along with a parameter (a) to account for residual magnetization in the y axis due to the SL pulse (Eq. 1). R_1 ($1/T_1$) and R_2 ($1/T_2$) were determined using two-parameter nonlinear fits (Eqs. 2 and 3). For the inversion recovery data at 0.5 T, a three-parameter fit was applied to determine
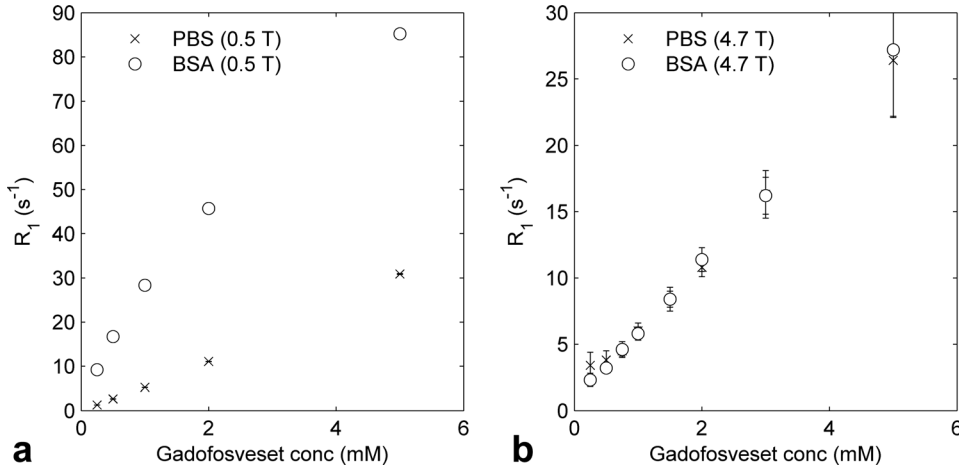
FIG. 1. R_1 values for gadofosveset in BSA (circles) and in PBS (crosses) at (**a**) 0.5 T and (**b**) 4.7 T. Error bars in (**a**) are smaller than data points.

S_0, R_1, and b, a parameter accounting for imprecision in the 180° inversion pulse angle (Eq. 4).

$$SI = S_0 . e^{-TSL.R1\rho} + a \qquad [1]$$

$$SI = S_0 . (1 - e^{-TR.R1}) \qquad [2]$$

$$SI = S_0 . e^{-TE.R2} \qquad [3]$$

$$SI = S_0 . (1 - b.e^{-TI.R1}) \qquad [4]$$

Confidence intervals were calculated at the 95% level. Datasets were compared for statistical significance at $\alpha = 0.05$ using a paired t-test in SPSS (v 16.0, IBM SPSS, NY).

RESULTS

Results are shown in Figs. 1–3, with error bars representing 95% confidence intervals. The overall R_1 values for solutions of gadofosveset in BSA and in PBS were significantly different at $B_0 = 0.5$ T ($P = 0.003$, Fig. 1a) but not different at 4.7 T ($P = 0.757$, Fig. 1b), confirming the lack of influence of binding on gadofosveset longitudinal relaxivity at high field strength. The $R_{1\rho}$ relaxation rates for solutions of gadofosveset in BSA at 4.7 T were significantly higher than for gadofosveset in PBS ($P = 0.001$, Fig. 2). PBS $R_{1\rho}$ values were similar to R_1 values at 4.7 T (BSA and PBS solutions; Fig. 1b). The $R_{1\rho}$ values for solutions of gadopentetate in BSA were similar to those for solutions of gadofosveset in PBS ($P = 0.380$, Fig. 2). R_2 values for solutions of gadofosveset in BSA and in PBS at 0.5 T displayed a similar pattern to R_1 values at this field strength, with significantly higher R_2 values for the BSA solutions ($P = 0.032$, Fig. 3a). R_2 values for equivalent solutions at 4.7 T were comparable with the R_2 values at 0.5 T and the $R_{1\rho}$ values at 4.7 T, with the BSA R_2 values being significantly higher than the PBS R_2 values ($P < 0.001$, Fig. 3b).

DISCUSSION

The high binding fraction of gadofosveset to SA differentiates it from other clinically approved Gd-based contrast agents. The influence of binding on R_1 is clear at 0.5 T (Fig. 1a) but is not observed at 4.7 T (Fig. 1b). Most clinical scanners operate at 3 T or lower, where an improve-

ment in longitudinal relaxivity of gadofosveset over other agents is still observed (8). However, as clinical field strengths continue to increase, this advantage of high relaxivity diminishes and an alternative method for exploiting gadofosveset characteristics would be of benefit. This study demonstrates the feasibility of a previously unpublished method for combining the albumin-binding properties of gadofosveset with the macromolecular sensitivity of SL to generate improved contrast modification at high field strengths. $R_{1\rho}$ values at 4.7 T for BSA solutions containing bound gadofosveset were found to be significantly greater than $R_{1\rho}$ values for PBS solutions containing unbound gadofosveset at the same concentration (Fig. 2).

Because of the sensitivity of the SL technique to macromolecules, it is not clear from these findings alone the extent to which the difference in $R_{1\rho}$ is attributable to the binding of gadofosveset or the presence of SA macromolecules. Comparison of $R_{1\rho}$ values for BSA and PBS solutions in the absence of contrast agent (0 mM) should give an indication of the influence of the albumin molecules on SL relaxation. However, the lengthy relaxation
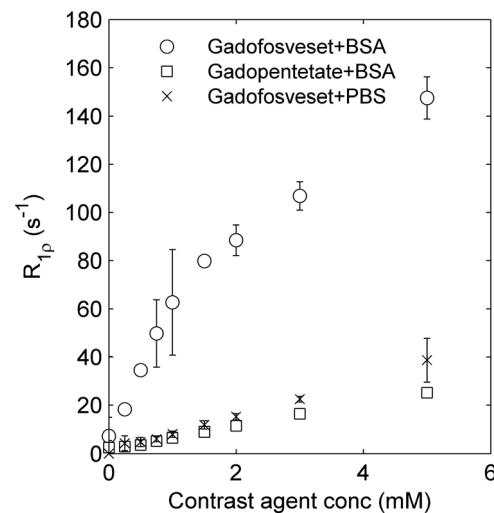

FIG. 2. $R_{1\rho}$ values for gadofosveset in BSA (circles) and in PBS (crosses) and gadopentetate in BSA (squares) at $B_0 = 4.7$ T, $B_{1L} = 90$ µT.
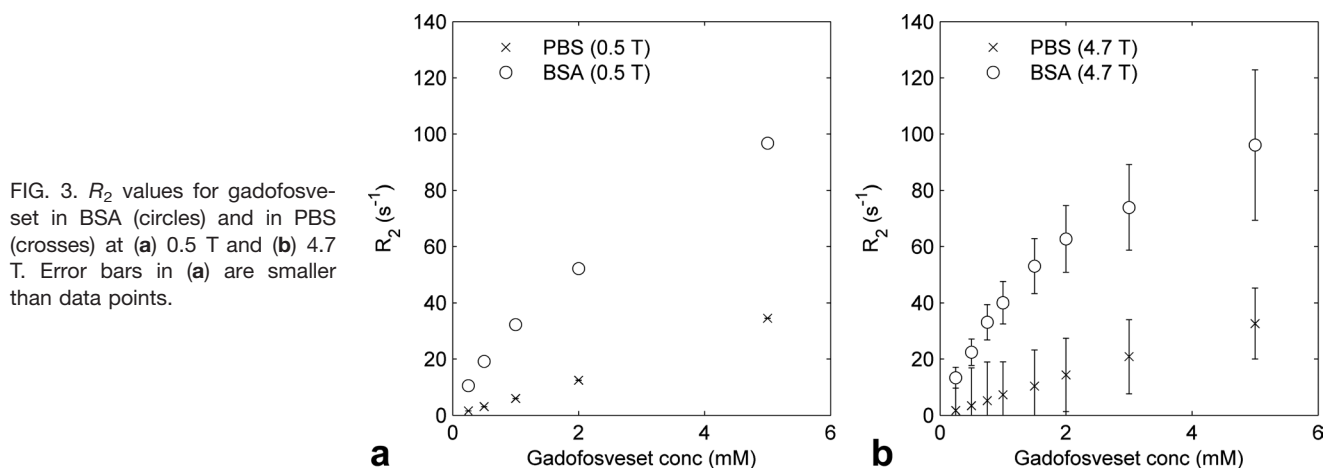
FIG. 3. R_2 values for gadofosveset in BSA (circles) and in PBS (crosses) at (**a**) 0.5 T and (**b**) 4.7 T. Error bars in (**a**) are smaller than data points.

times of these blank solutions led to poor model fits. Instead, the influence of albumin is better illustrated by measurements using the nonbinding contrast agent gadopentetate in BSA.

A previous study at contrast agent concentrations ≤ 0.5 mM (8) showed longitudinal relaxivity values at 4.7 T to be higher for gadofosveset in water than for gadopentetate in plasma (5.5 versus 3.7 mM^{-1} s^{-1}, respectively). If the SL relaxivity of gadopentetate in BSA is found to be higher than that of gadofosveset in PBS, this may be attributable to the BSA solution macromolecules. The $R_{1\rho}$ values for solutions of gadopentetate in BSA and gadofosveset in PBS (Fig. 2), and their associated relaxivity values, were not significantly different. The similarity of $R_{1\rho}$ values for gadofosveset in PBS and gadopentetate in BSA together with the observation of relatively large $R_{1\rho}$ values for gadofosveset in BSA all suggest, first, that the gadolinium has a greater effect on $R_{1\rho}$ than the mere presence of the macromolecule, and second, that it is the binding rather than any nonspecific interactions with the protein that has the largest effect on $R_{1\rho}$.

Although the SL contrast alteration observed with gadofosveset is not seen to the same extent with a small Gd-based nonbinding contrast agent in an equivalent macromolecular solution, SL has previously been successfully utilized in combination with nonbinding agents (14,17,19,20). The outcome of this study suggests that further benefit may be gained by exploiting the albumin-binding characteristics of an agent such as gadofosveset. In addition to increased $R_{1\rho}$ relaxation rates, the kinetic behavior of gadofosveset is modified by binding, resulting in a lower extravasation rate and longer excretion time (2). Measurements of R_1 at high field strength are unable to differentiate signal alteration from bound and free gadofosveset, due to their equivalent relaxivities. However, as $R_{1\rho}$ is substantially altered by binding, it may be possible to use these measurements to differentiate bound and free gadofosveset at high fields.

It should be noted that for this in vitro study it was not necessary to optimize SL imaging parameters to take into account potential tissue heating issues resulting from high SAR. A relatively high B_{1L} value of 90 μT was chosen to give improved image quality; although $R_{1\rho}$ increases as B_{1L} decreases, images become increasingly

susceptible to artifacts caused by magnetic field inhomogeneities at very low B_{1L} values (12). Methods for reducing SAR, such as off-resonance SL (25), were not explored. To avoid SAR-related constraints when carrying out in vivo measurements, an alternative, more practical solution may be to exploit the differences between bound and free gadofosveset transverse relaxation rates. T_2 values are routinely acquired on clinical scanners, and the effect of gadofosveset is clearly shown by R_2 values in the presence and absence of albumin at 4.7 T (Fig. 3b). For these in vitro solutions, both R_2 and $R_{1\rho}$ demonstrate greater relaxivity for bound gadofosveset than R_1. Although T_2 measurement may be considered more practical, several studies, in particular those looking at tumor response to cytotoxic treatment, have suggested that $T_{1\rho}$ may be a more responsive early indicator of physiological change than T_2 (15,16). It has also been suggested that improved (qualitative) tumor boundary definition may be achieved utilizing $T_{1\rho}$ rather than T_2 (26). A study of brain images in healthy volunteers at 1.5 T (27) found that $T_{1\rho}$-weighted images displayed improved spatial resolution over T_2-weighted images and $T_{1\rho}$ maps had a greater dynamic range than equivalent T_2 maps.

The scanning parameters at 4.7 T were optimized for physiological contrast agent concentrations. As a result, model fitting was less precise for the solutions containing the lowest and highest concentrations. The long T_1 values on the 0 mM solutions caused particular problems with model fitting and were excluded from this analysis. In addition, the PBS R_2 values at 4.7 T were based on a model fit to just three TE points, rather than the six points used for the BSA solutions, leading to greater imprecision in the calculated PBS R_2 values.

For the purpose of this study, gadopentetate was assumed to be a nonbinding contrast agent, although there is some evidence to suggest that the chelate displays a weak tendency for binding to albumin (28). At the comparatively low SA concentration used here, however, the measured relaxation rates suggested little influence of albumin binding for gadopentetate and it may effectively be considered to be nonbinding.

In summary, this study has shown the $R_{1\rho}$ response to gadofosveset in SA at high fields to be significantly larger than to a conventional small-molecule Gd-based

contrast agent. This suggests that SL may be a viable method for regaining the T_1 relaxivity lost by gadofosveset at high fields and may also provide an opportunity for additional tissue characterization through the differentiation of bound and free gadofosveset molecules. Despite offering potential benefits, implementation of this method in a SAR-limited clinical setting would require further investigation of optimal SL parameters prior to assessment in humans.

ACKNOWLEDGMENTS

REFERENCES

1. Aime S, Caravan P. Biodistribution of gadolinium-based contrast agents, including gadolinium deposition. J Magn Reson Imaging 2009;30:1259–1267.
2. Lauffer RB, Parmelee DJ, Dunham SU, Ouellet HS, Dolan RP, Witte S, McMurry TJ, Walovitch RC. MS-325: albumin-targeted contrast agent for MR angiography. Radiology 1998;207:529–538.
3. Caravan P, Cloutier NJ, Greenfield MT, McDermid SA, Dunham SU, Bulte JWM, Amedio JC Jr, Looby RJ, Supkowski RM, Horrocks Jr WD, McMurry TJ, Lauffer RB. The interaction of MS-325 with human serum albumin and its effect on proton relaxation rates. J Am Chem Soc 2002;124:3152–3162.
4. Eldredge HB, Spiller M, Chasse JM, Greenwood MT, Caravan P. Species dependence on plasma protein binding and relaxivity of the gadolinium-based MRI contrast agent MS-325. Invest Radiol 2006;41:229–243.
5. Barrett T, Kobayashi H, Brechbiel M, Choyke PL. Macromolecular MRI contrast agents for imaging tumor angiogenesis. Eur J Radiol 2006;60:353–366.
6. Bremerich J, Bilecen D, Reimer P. MR angiography with blood pool contrast agents. Eur Radiol 2007;17:3017–3024.
7. Muller RN, Raduchel B, Laurent S, Platzek J, Pierart C, Mareski P, Vander Elst L. Physicochemical characterization of MS-325, a new gadolinium complex, by multinuclear relaxometry. Eur J Inorg Chem 1999:1949–1955.
8. Rohrer M, Bauer H, Mintorovitch J, Requardt M, Weinmann H-J. Comparison of magnetic properties of MRI contrast media solutions at different magnetic field strengths. Invest Radiol 2005;40:715–724.
9. Caravan P, Farrar CT, Frullano L, Uppal R. Influence of molecular parameters and increasing magnetic field strength on relaxivity of gadolinium- and manganese-based T_1 contrast agents. Contrast Media Mol Imaging 2009;4:89–100.
10. Sepponen RE, Pohjonen JA, Sipponen JT, Tanttu JI. A method for T_1-rho imaging. J Comput Assist Tomogr 1985;9:1007–1011.
11. Redfield AG. Nuclear magnetic resonance saturation and rotary saturation in solids. Phys Rev 1955;98:1787–1809.
12. Martirosian P, Rommel E, Schick F, Deimling M. Control of susceptibility-related image contrast by spin-lock techniques. Magn Reson Imaging 2008;26:1381–1387.
13. Santyr GE, Henkelman RM, Bronskill MJ. Spin locking for magnetic-resonance imaging with application to human-breast. Magn Reson Med 1989;12:25–37.
14. Aronen HJ, Abo Ramadan U, Peltonen TK, Markkola AT, Tanttu JI, Jääskeläinen J, Häkkinen A-M, Sepponen R. 3D spin-lock imaging of human gliomas. Magn Reson Imaging 1999;17:1001–1010.
15. Duvvuri U, Poptani H, Feldman M, Nadal-Desbarats L, Gee MS, Lee WMF, Reddy R, Leigh JS, Glickson JD. Quantitative T_1 rho magnetic resonance imaging of RIF-1 tumors in vivo: detection of early response to cyclophosphamide therapy. Cancer Res 2001;61:7747–7753.
16. Kettunen MI, Sierra A, Narvainen MJ, Valonen PK, Yla-Herttuala S, Kauppinen RA, Grohn OHJ. Low spin-lock field T_1 relaxation in the rotating frame as a sensitive MR imaging marker for gene therapy treatment response in rat glioma. Radiology 2007;243:796–803.
17. Muthupillai R, Flamm SD, Wilson JM, Pettigrew RI, Dixon WT. Acute myocardial infarction: tissue characterization with T_1(rho)-weighted MR imaging—initial experience. Radiology 2004;232:606–610.
18. Borthakur A, Sochor M, Davatzikos C, Trojanowski JQ, Clark CM. T_1(rho) MRI of Alzheimer's disease. Neuroimage 2008;41:1199–1205.
19. Dixon WT, Oshinski JN, Trudeau JD, Arnold BC, Pettigrew RI. Myocardial suppression in vivo by spin locking with composite pulses. Magn Reson Med 1996;36:90–94.
20. Taylor C, Carballido-Gamio J, Majumdar S, Li XJ. Comparison of quantitative imaging of cartilage for osteoarthritis: T_2, T_1 rho, dGEMRIC and contrast-enhanced computed tomography. Magn Reson Imaging 2009;27:779–784.
21. Cobb JG, Xie J, Gore JC. Contributions of chemical exchange to $T_{1\rho}$ dispersion in a tissue model. Magn Reson Med 2011;66:1563–1571.
22. Rommel E, Kimmich R. T_1-rho dispersion imaging and volume-selective T_1-rho dispersion weighted NMR-spectroscopy. Magn Reson Med 1989;12:390–399.
23. Henkelman RM. Measurement of signal intensities in the presence of noise in MR images. Med Phys 1985;12:232–233.
24. Engelhardt RT, Johnson GA. T_1 rho relaxation and its application to MR histology. Magn Reson Med 1996;35:781–786.
25. Santyr GE, Fairbanks EJ, Kelcz F, Sorenson JA. Off-resonance spin locking for MR-imaging. Magn Reson Med 1994;32:43–51.
26. Poptani H, Duvvuri U, Miller CG, Mancuso A, Charagundla S, Fraser NW, Glickson JD, Leigh JS, Reddy R. T_1(rho) imaging of murine brain tumors at 4 T. Acad Radiol 2001;8:42–47.
27. Borthakur A, Wheaton AJ, Gougoutas AJ, Akella SV, Regatte RR, Charagundla SR, Reddy R. In vivo measurement of T1rho dispersion in the human brain at 1.5 tesla. J Magn Reson Imaging 2004;19:403–409.
28. Wang Y, Spiller M, Caravan P. Evidence for weak protein binding of commercial extracellular gadolinium contrast agents. Magn Reson Med 2010;63:609–616.